On The Coherent Dynamics of Turbulent Junction Flows

Joongcheol PAIK, Cristian ESCAURIAZA, Fotis SOTIROPOULOS

Saint Anthony Falls Laboratory, University of Minnesota

Mississippi River at 3rd Avenue SE Minneapolis, MN 55414 USA

Abstract. This study seeks to explore the unsteady nature of the turbulent horseshoe vortex (HSV) system at various Reynolds numbers (Re) through a series of detached eddy simulations (DES) of flows past three different wall-mounted obstacles: 1) a wing-shaped cylinder at Re = 115000; 2) a circular cylinder at Re = 39000 and 3) two cubes at Re = 22000 which were experimentally investigated by Devenport and Simpson [J. Fluid Mech., Vol. 210, p.23, 1990], Dargahi [Exp. Fluids, V. 8, p.1, 1989] and Martinuzzi and Havel [J. Fluids Eng., V. 122, p.24, 2000], respectively. Numerical simulations reproduce most experimental observations with good quantitative accuracy in terms of mean flows and turbulent statistics. For all cases considered the simulations capture the distinct bimodal evolution of the HSV system due to the quasiperiodic interplay between an organized state and a disorganized state. Double-peaked bimodal histograms of the velocity fluctuations are reproduced between the primary HSV and the flat wall for all cases, which is shown to be due to the strong interaction of the HSV with the wall causing the eruption of wall vorticity of positive sign. Our numerical results confirm that the dynamics of the turbulent HSV system is strongly dependent on the thickness of the approach boundary layer.

Key words: horseshoe vortex, junction flow, bi-modal, turbulence, DES.

1. Introduction

The turbulent boundary layer (BL) approaching a wall-mounted obstacle experiences an adverse pressure gradient and undergoes three-dimensional separation leading to the formation of a dynamically rich horseshoe vortex (HSV) system wrapping around the obstacle. Junction flows past wall mounted obstacles are encountered in many applications of practical interest in hydrodynamics, hydraulics, and aerodynamics and for that reason they have attracted considerable attention both experimentally and computationally. Various generic junction configurations that have been studied so far, including circular cylinders[3], wall mounted wings [4] and cubes [6, 7].
Experimental evidence has revealed the complex dynamics of the junction flows produced by the interaction of the turbulent BL with the pressure distribution in the vicinity of the wall-mounted obstacles. Early observations by Castro and Robins[2] showed that the global flow characteristics such as the size, the location and the intensity of the HSV are dependent on the thickness of incoming BL. For thick turbulent BL flows [3, 4, 7], the oscillating behavior of the HSV system is bimodal and

quasiperiodic which is characterized by double-peaked histogram of velocity fluctuations in the HSV region. For thin laminar BL[6], on the other hand, the structure of the upstream separation is characterized by multiple eddies upstream of the horseshoe vortex [6].
There are few unsteady numerical studies of the turbulent HSV system unlike the visualization and experimental measurements. The primary challenges to numerically simulating the coherent structures in junction flows stem from the complex geometrical configurations and the lack of practical coherent-structure resolving turbulence models for high Re simulations. In this study, multi-connected geometries are handled using the domain-decomposition approach with Chimera overset grids which is uniquely suited for the efficient clustering of the grid nodes in the region of interest as well as the boundary-fitted structured grid generation of very complex geometries. In our preliminary study, the unsteady Reynolds-averaged Navier-Stokes (URANS) solutions using conventional turbulence models appeared to fail to capture the rich dynamics of the HSV system. Although large eddy simulation (LES) has become an important tool for the turbulent flow simulation in engineering applications, the computational resource requirements of full wall-resolving LES at practical Re is still too high. We carried out detached eddy simulation (DES), a hybrid approach between URANS and LES proposed by Spalart et al.[11], for flows past three different wall-mounted obstacles: a wing-shape cylinder at Re = 115000; a circular cylinder at Re = 39000 and two cubes at Re = 22000 which were experimentally investigated by Devenport and Simpson[4], Dargahi[3] and Martinuzzi and Havel[6], respectively. The computed results are analyzed to numerically investigate the rich large-scale coherent dynamics of the HSV system in turbulent junction flows.

2. Numerical Method

The governing equations for the mean flow are the three-dimensional, unsteady, incompressible, Reynolds-averaged Navier-Stokes (RANS) equations. The detached-eddy simulation (DES) is a hybrid URANS/LES approach proposed by Spalart *et al.* [11]. To alleviate the well known shortcoming of the standard DES; namely that of premature, laminar-like flow separation we employ an adjusted DES model [8] to ensure that a URANS layer is always present near the wall regardless of the local grid spacing. The governing equations transformed in the generalized curvilinear coordinates and formulated in strong-conservation form are solved using a dual-time-stepping artificial compressibility (AC) iteration scheme. The AC form of the governing equations is discretized using a second-order-accurate finite-volume method on a non-staggered computational grid. The convective terms are discretized using the second-order accurate, upwind biased QUICK scheme, and central differencing is employed for other terms. The physical time derivatives are discretized with three-point-backward, Euler-implicit temporal-integration scheme. The system of equations is integrated in pseudo time using the pressure-based implicit preconditioner[10] enhanced with local-time-stepping and V-cycle multigrid acceleration. The complex wing geometry is handled using the domain-decomposition approach with structured, overset (chimera) grids. We apply a set of characteristics-based, non-reflecting boundary conditions at the outlet of the computational domains. The numerical method has been extensively evaluated for calculating various turbulent shear flows in complex geometrical configurations[9, 10, 8]. For a detailed description of the governing equations and of the numerical method the reader is referred to Paik *et al.* [10]. The code has been parallelized with MPI and run on a high performance computing cluster in the University of Minnesota Supercomputing Institute.

3. Results and Discussions

3.1. Flow past a wall-mounted wing

The numerical simulation is carried out for the flow past the wall-mounted cylindrical wing configuration studied experimentally by Devenport and Simpson[4] at Reynolds number $\mathrm{Re} = 1.15 \times 10^5$, based on the maximum thickness T and the approach bulk velocity. The inflow boundary is placed at $x/T = -18.24$ where the BL is prescribed using the experimental measurements [4]. The outlet boundary is placed at $x = 14.254T$ while both lateral boundaries and the boundary parallel to the bottom wall are placed at $z = \pm 3.5T$ and at $y = 3T$, respectively. No-slip boundary conditions are applied on the bottom wall and the wing surface. The computational domain is discretized using domain decomposition with 5 overset grids with a total active grid nodes of 6.2×10^6. The first grid node off of all solid walls is located at $y^+ \leq 0.5$. The simulation is carried out using a non-dimensional physical time step of $\Delta t = 0.007$ for a total of 30000 time steps.
To identify the coherent dynamics of the HSV system, we employ the so-called q-criterion[5]. As shown in Fig. 1(*right*), the flow around the wing is dominated by the very complex HSV system created by the roll up of the incoming flow due to the adverse pressure gradient. At the time instant shown in the figure the resulting vortical structure consists of at least two necklace-like vortices wrapping around the wing. Their mutual interaction as well as their interaction with the surrounding walls give rise to very complex flow patterns with at least two rows of hairpin vortices forming around the legs of the HSV system and in the region between the HSV and the surface of the wing. The inset in Fig. 1(*right*) shows probability density function (PDF) of the resolved streamwise velocity in the bimodal region underneath of the mean HSV core which is in close agreement with the experiments[4].
The measured[4] mean spanwise vorticity field and the mean streamlines at the plane of symmetry in the junction region (see the left upper figure in Fig. 2) reveals a number of distinct features of the mean HSV including an approximately elliptical in shape vortex core of negative vorticity, a double layer of negative vorticity upstream of the mean HSV and a thin layer of positive vorticity underneath the mean HSV. One of key findings in the experiments[4] is the presence of a pocket of intense turbulence kinetic energy (TKE) production in the junction region, as shown in Fig. 2(*right*). The measured contours reveal the presence of an elongated pocket of intense positive TKE production in the vicinity of the HSV with a long, thin tail stretching upstream above and parallel to the wall. It is clearly evident that the TKE production inside the BL is one order of magnitude lower than that produced in the HSV core region. Another important feature of the laboratory flow is the existence of a pocket of intense negative production between the positive pocket and the wall. Interestingly a similar feature was reported in a recently published DNS[12] of low Reynolds number flow past a wall-mounted cube. The calculated contours exhibit essentially all experimental features both qualitatively and quantitatively, except the location of the mean HSV core. It is important to emphasize that even though the simulated flow separates somewhat earlier than in the experiment, the calculated flowfield exhibits essentially all experimental trends both instantaneously and on average.
The flow structures in the junction region are very dynamic due to the continuous interplay between the backflow and zero-flow modes. An important feature of the HSV at backflow stage shown in Fig. 3(*left*) is the growth and propagation of disturbances along the coherent HSV core. The disturbances are marked by the distinct knot-like pattern that develop along the vortex core at several locations and their emergence triggers the subsequent instability. The instability originates in the region between the outer turn of the HSV and

the bottom wall and is marked by the emergence of multiple hairpin like vortices as seen in Fig. 3(*center*). The hairpins originate underneath the HSV and their legs are oriented perpendicular to the HSV core and stretched along the wall in the streamwise direction. As the hairpin vortices engulf the HSV they disorganize it rapidly, essentially grinding it up, and cause it to retreat downstream closer to the wing as shown in Fig. 3(*right*). As the destruction of the HSV is completed a new coherent vortex core begins to emerge upstream of the wing. Note that the formation of a new coherent vortex is essential as the approach BL continues to experience and can not sustain the imposed adverse pressure gradient and should roll up again and separate to form the HSV. The physical mechanizm leading to the formation of the hairpins is discussed in detail in Paik *et al.*[8] where we argue that the instability is contrifugal in nature.

To further elucidate the bi-modal nature of the HSV we analyze the streamwise velocity fluctuations at the plane of symmetry with proper orthogonal decomposition (POD). Fig. 4(*left*) shows the relative magnitude of the 12 largest eigenvalues λ_j of the decomposition, which represent the energy contained in each POD mode. It is clearly evident in this figure that the first two POD modes reproduce most of the variance of the velocity fluctuations, containing 85% of the streamwise turbulence kinetic energy. We compare in Fig. 4(*center*) the original streamwise velocity fluctuation times series at a point within the HSV with its POD reconstruction using only the first two POD modes. It shows that the POD reconstruction can capture in detail the most significant time scales and features of the flow, including the highly intermittent positive excursions in a region of negative average streamwise velocity. The respective power spectral densities of the first two modes are depicted in Fig. 4(*right*) and clearly show the existence of a dominant frequency for each mode. These frequencies are incommensurate, which, along with the fact that all essential dynamics is captured by the first two dominant POD modes, points to the conclusion that the coherent HSV dynamics is quasi-periodic.

3.2. Flow past a wall-mounted circular cylinder

We carry out numerical simulations of the HSV around a wall-mounted circular cylinder in a channel at a Reynolds number of Re=39000, based on the diameter of the cylinder D and the bulk velocity of the flow[3]. Through hydrogen bubble visualizations Dargahi[3] reported an intricate pattern of vortices being shed quasi-periodically from the point of separation upstream of the cylinder. A qualitative description of the HSV dynamics at the symmetry plane revealed somewhat different dynamics compared with that in the wing-body junction flow[4]. The HSV consists of a complex sequence of vortex formation and merging, with two major prevalent vortices in front of the cylinder. Turbulence statistics and oscillation frequencies of the HSV were estimated between 0.1 and 2.0 Hz, with values of turbulence intensity one order of magnitude larger at the HSV location.

The computational domain considers the geometry of the channel extending $7.5D$ upstream of the cylinder, as shown in Fig. 5(a). The domain is discretized by 5 overlapping blocks of a total of 7.2×10^6 grid nodes. The nodes are selectively clustered around the pier, with the two blocks around the cylinder containing 80% of the total nodes. The flow-field and turbulence variables at the inlet are calculated in a separate RANS simulation for steady developed flow in the rectangular channel considered in the experiments[3]. The small Froude number of the flow (Fr=0.2), allow us to consider a zero-gradient boundary condition at the free surface. No-slip boundary conditions are prescribed at all solid walls. The instantaneous vortical structures around the cylinder visualized with q iso-surfaces shown in Fig. 5(b) reveals two large necklace-like structures wrapping around the cylinder.

These structures experience a complex quasi-periodic interaction characterized by the development of hairpin vortices that appear at different times in each vortex. This process is essentially identical to the vortex evolution in the wing-body junction flow considered in the previous section, except a distinctive two-vortex system.
A sequence of instantaneous spanwise vorticity at the symmetry plane is shown in Fig. 6 to clarify the time-evolution of the multiple vortices of the HSV. Two primary clockwise vortices in front of the cylinder are the dominant structures sustained in time. The vortex nearer to the leading edge of the cylinder is very unstable and disorganized, while the upstream vortex, which has been recently shed from the point of separation in Fig. 6(a), grows stronger. Right before the upstream vortex becomes unstable, the two vortices merge producing a large structure that moves slowly toward the cylinder and develops hairpin vortices in its outer region (see Fig. 6(b)). Similar to the wing case, the instability leads to a strong eruption of near-wall fluid away from the wall, as shown in Fig. 6(c), which is initiated by the interaction of the HSV with the wall. The remnants of the vortex after the eruption reorganize in the downstream structure that appears closer to the cylinder, whereas a new upstream vortex emerges from the separation zone to repeat the process. Figs. 7(a) and 7(b) show the pdf and the spectrum of streamwise resolved velocity fluctuations at a point inside the HSV region. The histogram is clearly bimodal and consistent with the *back-flow* and *zero-flow* modes observed in the wing-body junction flow[4]. The computed spectrum exhibits dominant frequencies at 0.17, 0.25, and 0.32 Hz, which are in the range of values measured by Dargahi[3].

3.3. Flow past two wall-mounted cubes in tandem

Numerical simulation is carried out for one of the configurations investigated experimentally by Martinuzzi and Havel[6]. Two cubes of the height H are mounted with spacing $S/H = 2$ on a flat plate along the streamwise line of symmetry at a distance of $2H$ from the leading edge of the plate. Fig. 8(*left*) shows the computational overset grids consisting of a total of 12 subdomains to efficiently ensure fine grid resolution in the regions of interest with a total of 2×10^6 grid nodes. The outlet is placed at $x = 10H$ downstream of the leading edge of the first cube. Both lateral boundaries are placed symmetrically at $z = \pm 3.25T$ while boundary parallel to the bottom wall is placed at $y = 3.5T$. No-slip boundary conditions are applied on the plate and the cube surface. The experiments[6] show that the inlet profile is uniform within 1% of the freestream velocity and the turbulence intensity was less than 1.5%. To trigger the resolved turbulence in the numerical simulation, we employ the unsteady inflow conditions with homogeneous turbulent fluctuations of 1% turbulence intensity reproduced by the synthetic turbulence generation technique [1]. The Reynolds number based on H and the free-stream velocity is 22000. The oncoming BL is thin, laminar and matched the Blasius profile[6].
Fig. 8(*right*) shows a representative instantaneous snapshot of q-criterion in the entire domain. This figure along with our video files generated using instantaneous snapshots shows that the flow is dominated by the very complex vortical interactions in various regions: 1) the HSV system characterized by multiple vortices shed upstream of the leading edge; 2) the shear layer along the side and top edges of both cubes; 3) recirculating regions in the cube wakes; 4) periodic, low-frequency wake oscillations. The overall unsteady flow features are in good agreement with the experimental observations[6].
Martinuzzi and Havel[6] reported that the HSV system consists of a complex structure with at least two additional counter-rotating vortices upstream of the primary HSV. Due to the coarse measurement resolution, the presence of the secondary vortices is not clear in

the measured[6] vector plot shown in Fig. 9(a) but dimly discernible in the region upstream of the primary HSV near the plate. Though it appears to slightly underestimate the size of the primary HSV, our numerical simulation reproduces the overall features of the measured mean flow with reasonable accuracy. The smoke visualization[6] shown in Fig. 9(c) clearly depicts that the incoming flow separates from the saddle point of separation roughly at x =1.0. As shown in Fig. 9(d), It is captured in the numerical solutions with good accuracy. Fig. 9(d) also depicts the existence of a thin layer of positive vorticity between the mean HSV and the bottom wall of which overall shape is comparable to those in the turbulent BLs considered in previous applications. It is obviously evident from Fig. 9(d) showing the double-peaked histogram for the streamwise velocity fluctuations that a bimodal region exists between the primary HSV and the bottom wall in the thin laminar BL, similarly in the turbulent BL. Interestingly, our results are consistent with a recent study of Yakhot *et al.*[12] who carried out DNS for the flow past a wall mounted cube at a low Re = 5610 and captured the eruption of wall vorticity of positive sign and a bimodal distribution for the normal-to-the-wall velocity in the vicinity of the cube's front face.

To illustrate the unsteady flow features of the HSV system, we show in Fig. 10 a series of snapshots of instantaneous vorticity contours at the plane of symmetry. Fig. 10(*left*) depicts an organized HSV system characterized by distinct vortical structures including a strong primary HSV of negative vorticity near the lead edge and multiple vortices which continuously shed from the point of separation, move to downstream and merge with the primary HSV in the junction region. Fig. 10(*center*) shows vortical structures at an instant when the primary HSV is disorganized and the junction corner is occupied by the transported secondary vortices. For brief time intervals during the disorganized state, the HSV system is dominated by a long flat layer of negative vorticity and secondary vortices shedding further downstream , as shown in Fig. 10(*right*). Time series at two selected locations inside th boundary layer (see Fig. 9(d) for the locations), as shown in Fig. 11(a)(b), demonstrates that the streamwise velocity fluctuations at both locations are characterized by an aperiodic combination of two distinct states – namely organized and disorganized – with different amplitudes of the fluctuations. During the organized state, both streamwise velocity components appear to oscillate in a rather periodic manner at a dominant frequency of roughly 1.13 as shown in Fig. 11(c). On the other hand, a dominant frequency (roughly 0.1) has been reproduced at the low-frequency regime which presumably corresponds to low-frequency bimodal nature of the HSV system. We can not directly confirm the computed dominant frequency through the comparison with the measurements[6] due to the lack of the measurements[6] in this region. However, it is worth to point out here that the dominant frequency of about 0.1 coincides with the frequency detected in the vicinity of the mean HSV core reproduced by DNS[12] at a low Re.

4. Conclusions

We carried out DESs of flows past three different wall-mounted obstacles which were experimentally investigated by other researchers[3, 4, 6] at Reynolds number in the turbulent regime but for significantly different BL thicknesses, and reproduced with good accuracy the mean flows and turbulent statistics. Numerical simulations captured most unsteady flow features of the HSV system observed in the experiments through various visualization techniques. The double-peaked histograms of velocity fluctuations – one of most important features – are captured numerically near the primary HSV in all three flows, in spite of the huge difference of BL thicknesses. This study confirms that the quasiperiodic bimodal nature of the HSV system is due to the strong interaction of the primary HSV with

the flat bottom wall in the relatively thick approach BL flows[3, 4] and the interactions of multiple vortices continuously shedding from the upstream saddle point of separation with the flat wall in the thin BL case[6].

Acknowledgments

This work was partly supported by NSF grant EAR-0120914 as part of the National Center for Earth-surface Dynamics. Computing resources are provided by the University of Minnesota Supercomputing Institute.

References

[1] P. Batten, U. Goldberg, and S. Chakravarthy. Interfacing statistical turbulence closures with large-eddy simulation. *AIAA J.*, 42(3):485–492, 2004.

[2] I. P. Carstro and A. G. Robins. The flow around a surface-mounted cube in unifor and turbulent streams. *J. Fluid Mech.*, 79:307–335, 1977.

[3] B. Dargahi. The turbulent flow field around a circular cylinder. *Exp. Fluids*, 8:1–12, 1989.

[4] W. J. Devenport and R. L. Simpson. Time-dependent and time-averaged turbulence structure near the nose of a wing-body junction. *J. Fluid Mech.*, 210:23–55, 1990.

[5] J. C. R. Hunt, A. A. Wray, and P. Moin. Eddies, stream, and convergence zones in turbulent flows. In *Proceeding of the Summer Program*, pages 193–208, Center for Turbulence Research, NASA Ames/Stanford Univ., 1988.

[6] R. Martinuzzi and B. Havel. Turbulent flow around two interfering surface-mounted cubic obstacles in tandem arrangement. *ASME J. Fluids Eng.*, 122:24–31, 2000.

[7] R. Martinuzzi and C. Tropea. The flow around surface-mounted, prismatic obstables placed in a fully developed channel flow. *ASME J. Fluids Eng.*, 115:85–92, 1993.

[8] J. Paik, C. Escauriaza, and F. Sotiropoulos. On the bimodal dynamics of the turbulent horseshoe vortex system in a wing-body junction. *Phys. Fluids*, 19(3):035110, 2007.

[9] J. Paik, L. Ge, and F. Sotiropoulos. Toward the simulation of complex 3D shear flows using unsteady statistical turbulence models. *Int. J. Heat Fluid Flow*, 25(3):513–527, 2004.

[10] J. Paik, F. Sotiropoulos, and M. J. Sale. Numerical simulation of swirling flow in a hydroturbine draft tube using unsteady statistical turbulence models. *ASCE J. Hydraul. Eng.*, 131(6):441–456, 2005.

[11] P. R. Spalart, W. H. Jou, M. Strelets, and S. R. Allmaras. Comments on the feasibility of LES for wings and on a hybrid RANS/LES approach. In C. Liu and Z. Liu, editors, *Advances in DNS/LES*. Greyden Press, Columbus Oh, Aug 4-8 1997.

[12] A. Yakhot, T. Anor, H. Liu, and N. Nikitin. Direct numerical simulation of turbulent flow around a wall-mounted cube: spatio-temporal evolution of large-scale vortices. *J. Fluid Mech.*, 566:1–9, 2006.

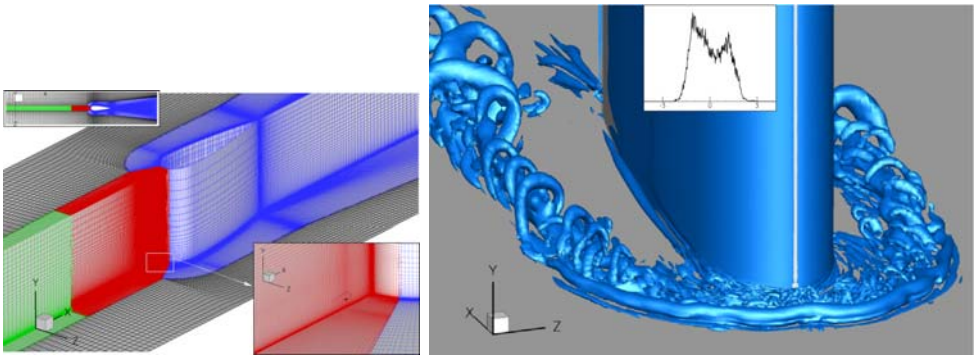

Figure 1. Flow near the wing-body junction: (*left*) overset grids and the coordinate system and (*right*) an instantaneous snapshot of 3D coherent structures identified by iso-surface of q-criterion ($q = 1$) where the insect shows the double-peaked histogram of streamwise velocity fluctuations computed at a point between the primary HSV and the bottom wall.

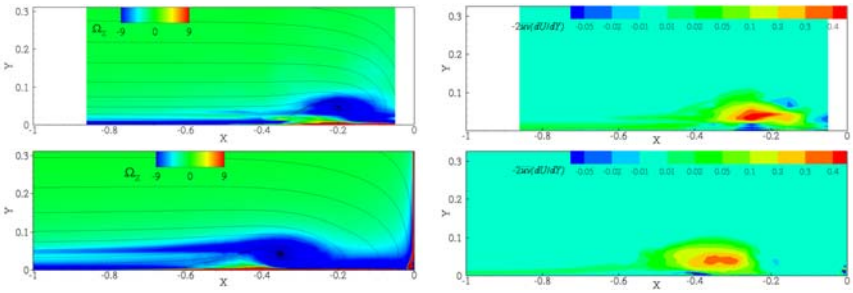

Figure 2. (*upper*) measured[4] and (*lower*) computed mean (*left*) vorticity distribution overlaid by streamlines and (*right*) turbulence production at the plane of symmetry.

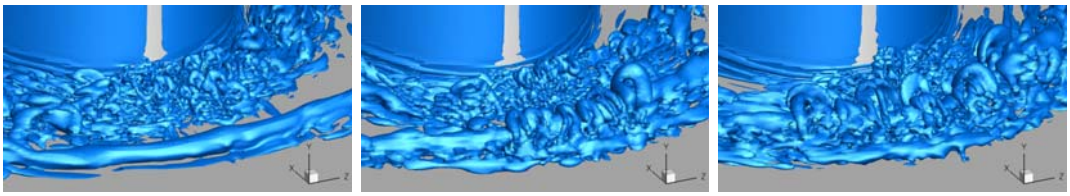

Figure 3. Instantaneous sequential snapshots of iso-surface of q-criterion near the leading edge depicting vortex evolution from (*left*) the backflow stat to (*right*) the zero-flow state.

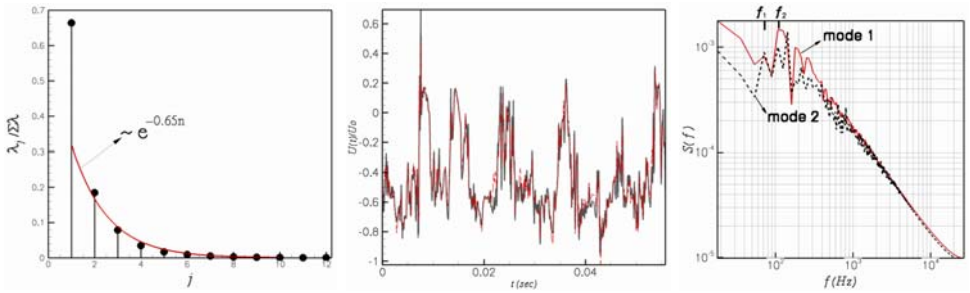

Figure 4. POD analysis of streamwise velocity component u computed underneath the mean HSV core: (*left*) 12 largest eigenvalues of the POD decomposition; (*center*) bimodal reconstruction of u (red line) compared to the original time series (black line); (*right*) power spectrum density of the autocorrelation functions of the first two modes.

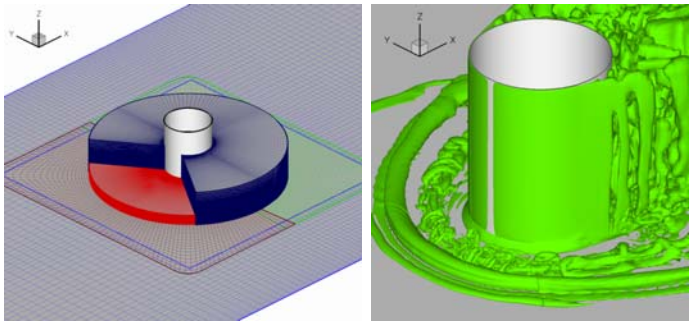

Figure 5. (*left*) Grid layout and (*right*) instantaneous q iso-surfaces for the flow past a surface-mounted cylinder at Re=39000 (Dargahi, 1989).

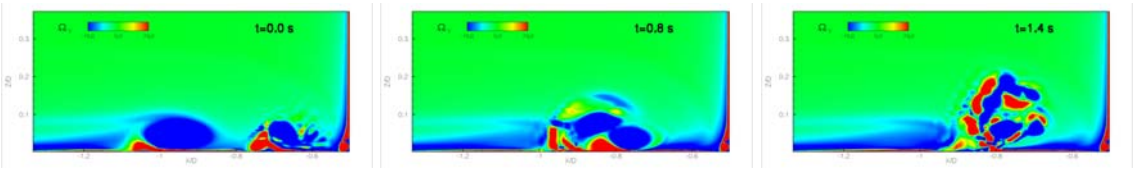

Figure 6. Evolution of the HSV system for the cylinder case. Sequence of vortex generation, merging, and eruption are depicted with the time. Contours indicate the out-of-plane vorticity.

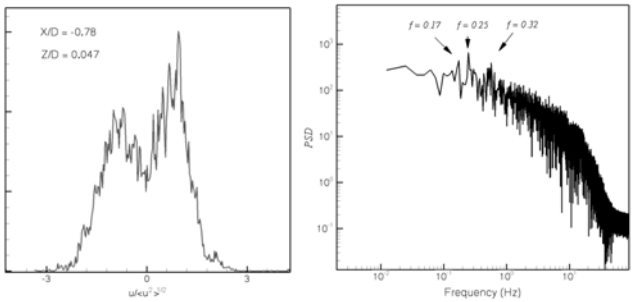

Figure 7. Time-series analysis of streamwise velocity fluctuations at a point inside the HSV system in the cylinder flow: (*left*) bimodal pdf indicates that the *back-flow* and *zero-flow* modes characterize the flow at the HSV and (*right*) power spectrum shows that low-frequency processes also dominate the dynamics at this region.

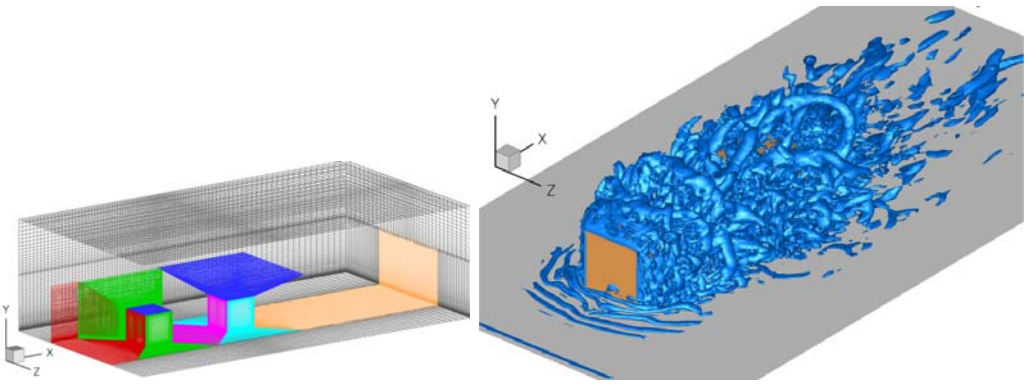

Figure 8. Flow past wall-mounted two cubes: (*left*) overset grids and the coordinate system and (*right*) a snapshot of instantaneous flow identified by iso-surface of $q = 4$.

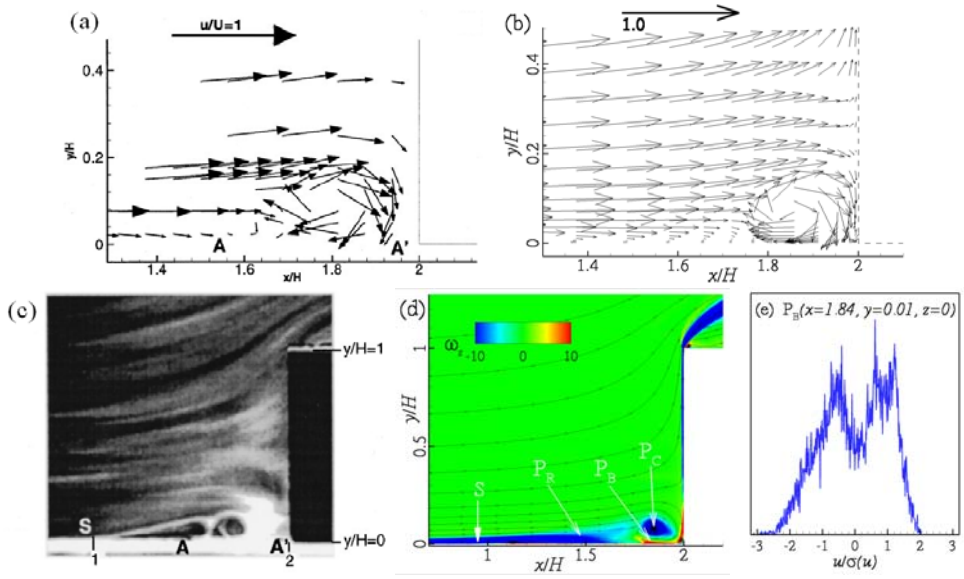

Figure 9. Comparison of the computed solutions with the measurements of Martinuzzi and Havel [5] at the plane of symmetry: (a) measured mean velocity vectors [5]; (b) computed time-averaged velocity vectors plotted on every 4th horizontal and every 2nd vertical nodes; (c) smoke visualization [5]; (d) time-averaged streamlines and out-of-plane vorticity contours; (e) histogram of streamwise velocity at the point P_B (see figure (d) for the location).

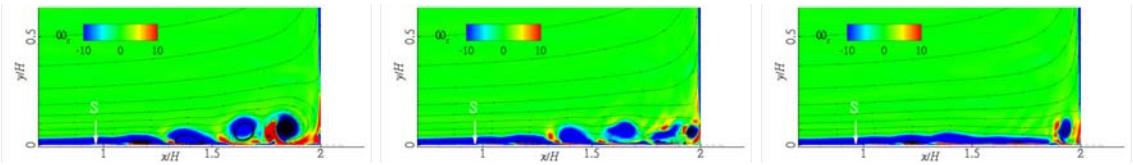

Figure 10. Evolution of the HSV system from the organized state to the disorganized one visualized by sequential (*left*-to-*right*) snapshots of instantaneous out-of-plane vorticity contours and streamlines.

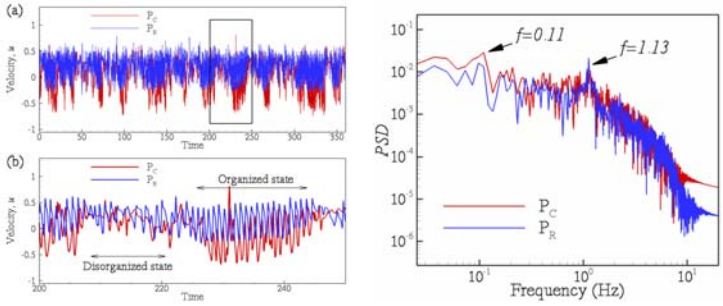

Figure 11. Temporal characteristics of streamwise velocity components computed at selected locations, P_C and P_R, (see Fig. 9(d) for the locations): (a) full time-series, (b) time series zoomed in a selected time period indicated by a rectangular box in figure (a); and (c) power spectral density.